# Mössbauer and photocatalytic studies of CaFe2O4 nanoparticle-containing aluminosilicate prepared from domestic waste simulated slag

ALI, AS, ISHIKAWA, S, NOMURA, K, KUZMANN, E, HOMONNAY, Z, SCRIMSHIRE, Alex <http://orcid.org/0000-0002-6828-3620>, BINGHAM, Paul <http://orcid.org/0000-0001-6017-0798>, KREHULA, S, RISTIĆ, M, MUSIĆ, S and KUBUKI, S



**Published version**

ALI, AS, ISHIKAWA, S, NOMURA, K, KUZMANN, E, HOMONNAY, Z, SCRIMSHIRE, Alex, BINGHAM, Paul, KREHULA, S, RISTIĆ, M, MUSIĆ, S and KUBUKI, S (2019). Mössbauer and photocatalytic studies of CaFe2O4 nanoparticle-containing aluminosilicate prepared from domestic waste simulated slag. Journal of Radioanalytical and Nuclear Chemistry.

**Copyright and re-use policy**

# Mössbauer and Photocatalytic Studies of $CaFe_2O_4$ Nanoparticles-Containing Aluminosilicate prepared from Domestic Waste Simulated Slag

Ali A. S.[1], Ishikawa S.[1], Nomura K.[1], Kuzmann E.[2], Homonnay Z.[2], Scrimshire A.[3], Bingham P. A.[3], Krehula S.[4], Ristić M.[4], Musić S.[4], Kubuki S.[1]

[1] *Graduate School of Science, Tokyo Metropolitan University, 1-1 Minami-Osawa, Hachi-Oji, Tokyo 192-0397, JAPAN*

[2]*Institute of Chemistry, Eötvös Loránd University, Pasmany P.s. 1/A, Budapest 1117, HUNGARY*

[3] *Faculty of Science, Technology and Arts, Sheffield Hallam University, Howard St., Sheffield S1 1WB, UK*

[4]*Division of Materials Chemistry, Ruder Bosković Institute, Bijenička c. 54, 10000 Zagreb, CROATIA*

## Abstract

The relationship between local structure and visible-light activated photocatalytic effect of simulated domestic waste slag glass-ceramics (R-NaWSFe) was investigated. The largest pseudo-first-order rate constant of $9.75 \cdot 10^{-3}$ $min^{-1}$ was estimated for methylene blue decomposition test under the visible-light irradiation using R-NaWSFe with additional 30 mass% of $Fe_2O_3$ heat-treated at 900 $^oC$ for 100 min. The reason for the high photoactivity of this sample was mainly due to nanoparticles of $CaFe_2O_4$ and $\alpha$-$Fe_2O_3$ confirmed by the Mössbauer spectrum measured at 77 K. It is concluded that the nanoparticles of magnetic components in silica are essential for exhibiting visible-light activated catalytic effect.

## Keywords

$^{57}$Fe Mössbauer spectroscopy, Photocatalytic effect, Visible-light, Nanoparticles, $CaFe_2O_4$, $\alpha$-$Fe_2O_3$,

## 1. Introduction

Treatments of waste materials and wastewater are serious environmental problems all over the world. The Organization for Economic Co-operation and Development (OECD) reported that the annual total amount of municipal waste discarded from the OECD affiliated countries was calculated to be $6.22 \cdot 10^{11}$ kg, corresponding to the disposal of 560 kg/person in 2007 [1]. These reported values concerning the amounts of waste materials are almost stable as compared with those recently reported values of $6.56 \cdot 10^{11}$ kg, corresponding 522 kg/person reported in 2013 [2]. As for the wastewater pollution in Japan, chemical oxidation demand (COD) achievement rate, which indicates the ratio of closed water system like pond or lake having the COD value less than the upper limitation of 8 mg $L^{-1}$ has been stable at around 55 % [3]. These statistics show that the no effective solutions for reducing the waste materials and for wastewater purification have been developed. Therefore, finding a new route for recycling solid waste as water purifying material is essential for solving serious environmental problems.

Our research group found that the glass-ceramics prepared from a domestic waste slag (WS), of which chemical component is $SiO_2$(38.4 mass%), CaO(28.5), $Al_2O_3$(14.9), $Fe_2O_3$(5.5), and others (12.7), collected at the incineration plant in Ube city, Yamaguchi, Japan, with additional $Fe_2O_3$ decreased the COD value from 250 to 36 mg $L^{-1}$ after 10 days [4]. We then reported that iron-containing soda lime silicate glass with the chemical composition of $15Na_2O \cdot 15CaO \cdot (70-x)SiO_2 \cdot xFe_2O_3$, abbreviated as NCFS*x*, with '*x*' of 50 (in mass%) decreased COD value of artificial drain from 280 to 55.2 mg $L^{-1}$ after 10 days with the pseudo-first-order rate constant ($k$) of $4.7 \cdot 10^{-1}$ $day^{-1}$[5]. These results implied that the iron-silicate glass-ceramics could be applied as a water purifying materials for decomposing organic compounds which causes an increase in COD.

In relation to the development of wastewater purifying materials from iron silicate glass-ceramics, NCFS*x* glass with '*x*' of 50 heat-treated at 1000 $^{o}$C for 100 min decomposed methylene blue (MB) in the aqueous solution with the *k* of $4.78 \cdot 10^{-4}$ $min^{-1}$[6]. The room temperature (RT) Mössbauer spectrum of the heat-treated NCFS*x* with '*x*' of 50 were composed of an magnetic sextet with an isomer shift ($\delta$) of 0.36 mm $s^{-1}$ and an internal magnetic field ($H_{int}$) of 51.8 T due to hematite ($\alpha$-$Fe_2O_3$) and a relaxed sextet with the $\delta$ and $H_{int}$ of 0.34 mm $s^{-1}$and 37.9 T, respectively, due to the iron oxide nanoparticles [6]. Further, a much larger *k* value of $9.26 \cdot 10^{-3}$ $min^{-1}$ was recorded for MB decomposition test using a heat-treated $15Na_2O \cdot 15CaO \cdot 40Fe_2O_3(30-x)SiO_2 \cdot xAl_2O_3$ glass, abbreviated as NCFSA*x* with '*x*' of 11[7]. Two magnetic sextets with $\delta$ and $H_{int}$ of 0.37 mm $s^{-1}$ and 51.2 T and 0.38 mm $s^{-1}$ and 52.4 T were observed from the RT Mössbauer spectrum of this sample [7].

Recently, a glass-ceramics prepared from $Na_2CO_3$, WS and $Fe_2O_3$, abbreviated as NaWSFe*x*, by melt-quenching method showed the *k* value of $2.65 \cdot 10^{-3}$ $min^{-1}$ when they were heat-treated at 800 $^{o}$C for 100 min [8]. The Mössbuer spectra measured at 77 K showed several sextets, one of which had $\delta$ and $H_{int}$ of 0.41 mm $s^{-1}$ and 52.7 T attributed to nanoparticles of $\alpha$-$Fe_2O_3$ [8]. These results show that the iron-containing silicates exhibit photocatalytic ability through the presence of $\alpha$-$Fe_2O_3$ and its analogous iron oxides at the nano-scale. However, it is difficult for NaWSFe*x* to precisely evaluate the visible light-activated photocatalytic effect of $\alpha$-$Fe_2O_3$ precipitated in the silica glass matrix because WS contains lots of impurity elements.

Therefore, in order to classify the chemical environment of iron oxides which causes the visible-light activated photocatalytic activity in the silica matrix, the relationship between visible-light activated catalytic effects and local structure of "*simulated"* domestic waste slag with different iron concentrations, abbreviated as R-NaWSFe*x* (*x* = 10, 30 and 50 mass% of $Fe_2O_3$ in the $Na_2O$-CaO-$SiO_2$-$Al_2O_3$-$Fe_2O_3$ system) was investigated by $^{57}$Fe-Mössbauer spectroscopy, X-ray diffractometry(XRD), and ultraviolet-visible light absorption spectroscopy(UV-Vis).

## 2. Experimental

Glass and ceramics produced from domestic waste model slag with different iron concentration, denoted as model-slag+10$Na_2O$+*x*$Fe_2O_3$, abbreviated as (R-NaWSFe*x*, *x* = 10, 30, 50 mass%) were prepared by melt quenching method. The chemical composition of the model slag was based on the previously reported values[8] except for minor components of the first transition metal oxides. Weighed amounts of $Na_2CO_3$ (Wako 199-01585), $CaCO_3$ (Wako 030-00385), $Fe_2O_3$ (Wako 096-04825), $Al(OH)_3$ (Wako 014-01925) and $SiO_2$ (Kanto Kagaku 37974-00) were mixed with an agate mortar. The mixture was put into a platinum crucible and melted at 1400 $^oC$ for 60 min in an electrical muffle furnace. Dark brown samples were obtained by dipping the crucible bottom into ice-cold water. The prepared glass and glass-ceramics were subjected to the following isothermal heat treatment for 100 min at 800 and 900 $^oC$. The estimated chemical composition of R-NaWSFe*x* is listed in Table 1.

**Table 1** The estimated chemical composition of R-NaWSFe*x* (in wt%)

| *x* | $Na_2O$ | CaO | $Al_2O_3$ | $SiO_2$ | $Fe_2O_3$ |
|---|---|---|---|---|---|
| 10 | 11.2 | 26.9 | 14.0 | 23.3 | 24.6 |
| 30 | 9.6 | 23.1 | 12.0 | 20.0 | 35.3 |
| 50 | 8.4 | 20.2 | 10.5 | 17.5 | 43.4 |

The prepared glasses and glass-ceramics containing model slag plus additions, before and after heat-treatment were characterized by X-ray diffractometry (XRD), $^{57}$Fe-Mössbauer spectroscopy and ultra-violet visible-light absorption spectroscopy (UV-VIS). The XRD patterns were measured in the $2\Theta$ range of 10 and 80 $^o$ with the sampling pitch of 0.02 $^o$ and scan speed of 5 $^o$ $min^{-1}$. The X-rays of Cu-$K_\alpha$ ($\lambda$ = 0.1541 nm) were generated by applying the voltage of 50 kV and the current of 300 mA. The recorded XRD patterns were identified by JCPDS cards by PDXL. Measurements of Mössbauer

spectra at room and liquid nitrogen temperatures (77 K) were carried out by conventional acceleration method using 925MBq $^{57}$Co(Rh) and α-Fe as a source and reference, respectively. For the measurement, 100 mg of well-pulverized sample is homogeneously dispersed on the transparent adhesive tape so that it was circular in shape with a diameter of 10 mm. The obtained spectra were fitted by Lorentzian lineshapes using Mosswinn 3.0i XP software. For the evaluation of visible-light activated photocatalytic ability, 20 mL of 20 μ mol $L^{-1}$ methylene blue aqueous solution ($MB_{aq}$) prepared from methylene blue (Wako 133-06962) was poured into a plastic vial together with 40 mg of powdered sample, and irradiated with the visible light with the wavelength of 420 – 700 nm emitted from a metal halide lamp with an output power of 100 W and intensity of 6 $mWcm^{-2}$ . The $MB_{aq}$ concentration after the catalytic reaction was determined by UV-VIS spectrometer under the wavelength range of 200 – 800 nm and a scan speed of 1 nm $sec^{-1}$.

## 3. Results and discussion

### 3.1 UV-VIS Spectra

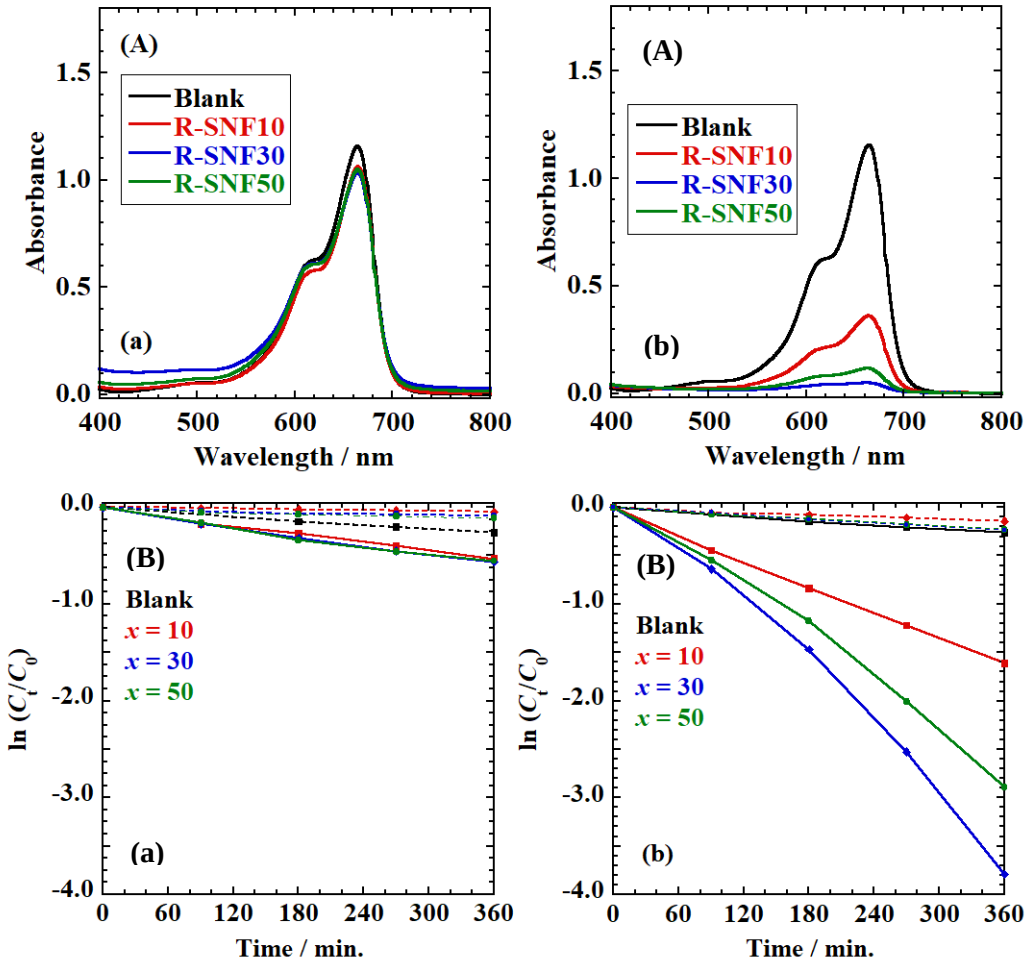


**Fig. 1** (A) UV–Vis spectra and (B) ln($C_t/C_0$) *vs. t* plot of $MB_{aq}$ reacted with R-NaWSFe*x* after heat treatment for 100 min. at (a) 800 and (b) 900 $^{o}$C

UV-Vis spectra of $MB_{aq}$ degradation test using R-NaWSFe*x* with '*x*' of 10, 30 and 50 heat-treated for 100 min at 800 and 900 $^{o}$C are shown in Fig. 1. We could confirm the maximum absorption wavelength at 664 nm due to the original MB from the UV-Vis spectra before the degradation test. The concentration of the $MB_{aq}$ was determined by the Lambert-Beer equation, *i.e.*,

$$A = \varepsilon_0 C_t l \quad (1)$$

where $A$, $\varepsilon_0$, $C_t$ and $l$ are absorbance determined at 664 nm, molar absorption coefficient (= 7.9 •$10^4$ $mol^{-1}$ $cm^{-1}$ L[9]), MB concentration after $t$ min [mol $L^{-1}$] and cell length (= 1 cm), respectively. When the $MB_{aq}$ was reacted in the dark with R-NaWSFe*x* with *x* of 10,

30 and 50 after heat-treated at 800 $^{o}$C for 100 min, almost constant MB concentration was recorded for the degradation test using all three samples as shown in the dotted lines in Fig. 1 (B) (a). On the other hand, a decrease in MB concentration was observed from 20.0 to 11.8, 11.4, and 12.8 μ mol $L^{-1}$ reacted under the visible-light with R-NaWSFe*x* having the '*x*' of 10, 30 and 50 for 360 min, respectively ( see Fig. 1 (B) (a)). However, the MB concentration after 360 min irradiation of visible-light was comparable to that of a blank test (12.8 μ mol $L^{-1}$). In contrast, remarkable decreases in MB concentration were observed from 20 to 4.00, 0.45, and 1.10 μ mol $L^{-1}$ by using R-NaWSFe*x* with '*x*' of 10, 30 and 50 heat-treated at 900 $^{o}$C, respectively ( see Fig. 1 (B) (b)).

A pseudo-first-order rate constant (*k*) is evaluated by the following equation, *i.e.*,

$$ln(C_t/C_0) = -kt \quad (2)$$

where $C_0$ is the initial MB concentration ( = 20 μ mol $L^{-1}$). In order to evaluate the photocatalytic ability of the studied samples, estimation of *k* values is carried out by plotting, $ln(C_t/C_0)$ vs. *t*, as shown in Fig. 1(B). Under visible-light irradiation, almost comparable *k* values of (1.48±0.02) •$10^{-3}$, (1.63±0.01) •$10^{-3}$ and (1.64±0.01)•$10^{-3}$ $min^{-1}$ were respectively obtained for R-NaSWFe*x* with '*x*' of 10, 30 and 50 heat-treated for 100 min at 800 $^{o}$C, which is slightly larger than that of blank value (= (1.20±0.01)•$10^{-3}$ $min^{-1}$). In contrast, much larger *k* values of (4.52±0.01) •$10^{-3}$, (9.75±0.01) •$10^{-3}$ and (7.59±0.01)•$10^{-3}$ $min^{-1}$ were estimated for the same samples heat-treated for 100 min at 900 $^{o}$C under the visible-light irradiation. These results indicate that R-NaWSFe*x* heat-treated at the higher temperature has a higher photocatalytic ability which depends on kinds and amounts of the precipitated crystalline phases. In our previous study, we could observe a *k* value of 2.65•$10^{-3}$ $min^{-1}$ for a glass-ceramics prepared from $Na_2O$+domestic waste slag+*x*$Fe_2O_3$ by melting at 1400 $^{o}$C for 1 h and heat-treated at 800 $^{o}$C for 100 min [8]. By comparing the largest *k* value obtained for R-NaWSFe30 heat-treated at 900 $^{o}$C in this study(=(9.75±0.01) •$10^{-3}$ $min^{-1}$) and that obtained for the glass-ceramics prepared from existing domestic waste slag(=2.65•$10^{-3}$ $min^{-1}$), it can be said that much more effective photocatalytic material can be prepared by isolating impurity from existing domestic waste slag.

### 3.2 XRD patterns

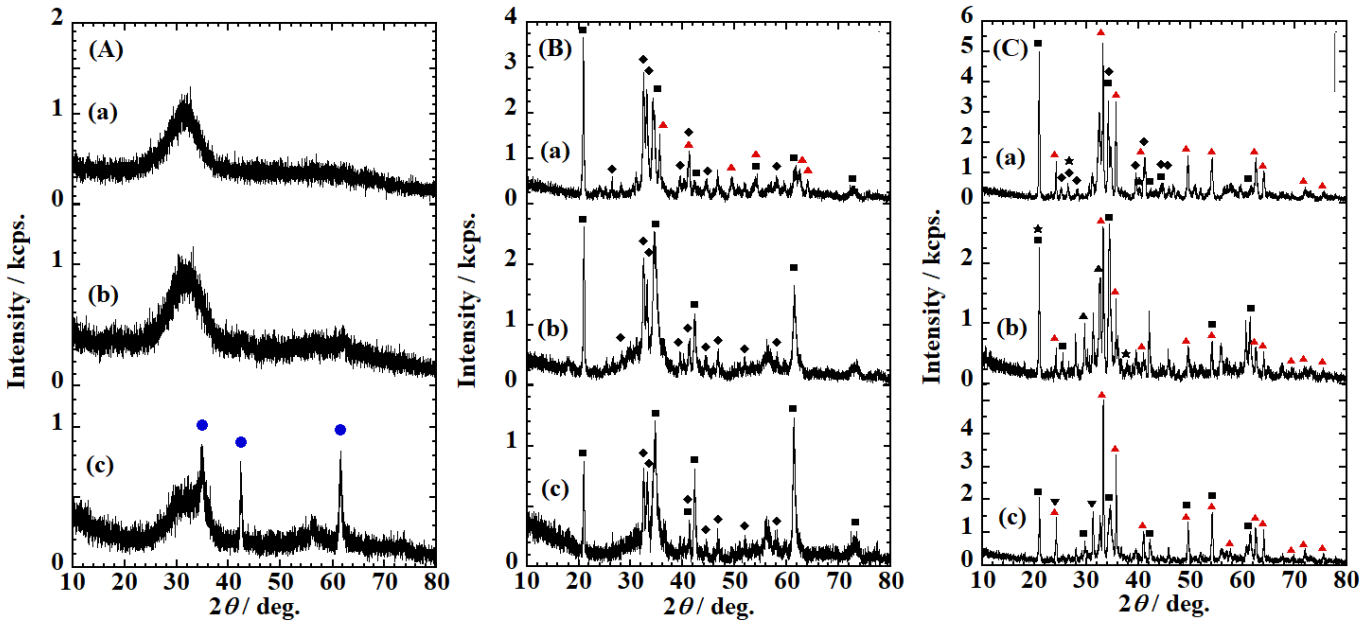


**Fig. 2** XRD patterns of R-NaWSFe*x* samples with '*x*' of (a)10, (b) 30 and (c) 50, (A) before and after heat treatment for 100 min at (B) 800 °C and (C) 900 °C. ●: γ-$Fe_2O_3$, ■: $NaAlSiO_4$, ◆: $Ca_2SiO_4$, ▲: α-$Fe_2O_3$, ▲: $Ca_3SiO_5$, ▼: $Ca_2Al_2SiO_7$, ★: $SiO_2$.

In Fig. 2, XRD patterns of R-NaWSFe*x* samples before and after heat treatment for 100 min at 800 °C and 900 °C are indicated. Before the heat treatment, we could confirm X-ray halo patterns which have a peak at $2\Theta$ of around 32.0° due to the amorphous structure for R-NaWSFe*x* samples with '*x*' of 10 and 30, whereas sharp intense peaks were detected at the $2\Theta$ of 34.8, 42.3 and 61.5° due to maghemite (γ-$Fe_2O_3$, PDF No. 01-076-4113) for R-NaWSFe50. The crystallite size (*D*) of compounds detected by the XRD patterns can be estimated by Sherrer's formula [10], *i.e.*,

$$D = K\lambda / \beta \cos\Theta \qquad (3)$$

where *K*, λ and $\beta$ are Sherrer's constant, wavelength of the X-ray(= 0.1541 nm) and full width at the half of maximum, respectively. Using the Sherrer's formula (3), the crystallite size of γ-$Fe_2O_3$ precipitated in R-NaWSFe50 was calculated to be (24±9) nm.

It should be noted that the thermal stability of R-NaWSFe*x* becomes higher because XRD pattern of glass-ceramics prepared from as collected domestic waste slag with similar chemical composition showed peaks due to the crystalline phase when it contains additional $Fe_2O_3$ of more than 30 mass%[8]. As for XRD patterns of R-NaWSFe*x* samples after heat-treatment at 800 $^oC$, crystalline phases of $NaAlSiO_4$ (PDF No. 00-011-0221) and $Ca_2SiO_4$ (PDF No. 01-086-0399) were identified in all samples, while $\alpha$-$Fe_2O_3$ (PDF No. 01-089-0599) can be identified only in the case of $x = 10$. After heat-treatment at 900 $^oC$, $\alpha$-$Fe_2O_3$ can be detected in all samples with additional phases of $SiO_2$ (PDF No. 01-089-8937) for $x = 10$ and 30, while for $x = 50$, $Ca_2Al_2SiO_7$ (PDF No. 01-075-1677) can be detected. The averaged crystallite sizes were respectively estimated to be $29 \pm 4$, $35 \pm 5$ and $25 \pm 3$ nm for $x = 10$, 30 and 50 heat-treated at 800 $^oC$, while they were $47 \pm 5$, $44 \pm 4$ and $41 \pm 3$ nm for 900 $^oC$ heat-treated samples. When we consider the differences in the $k$ values of $1.48\text{-}1.64 \bullet 10^{-3}$ $min^{-1}$ observed for $MB_{aq}$ degradation test using R-NaWSFe*x* heat-treated at 800 $^oC$ and those of $4.52 \bullet 10^{-3}$-$9.75 \bullet 10^{-3}$ $min^{-1}$ recorded by using samples afterheat-treated at 900 $^oC$, it can be considered that precipitation of $\alpha$-$Fe_2O_3$ phase is essential for exhibiting visible-light activated photocatalytic effect of heat-treated R-NaWSFe*x*.

## 3.3 $^{57}$Fe-Mössbauer Spectra

### 3.3.1 Room temperature (RT) $^{57}$Fe-Mössbauer Spectra

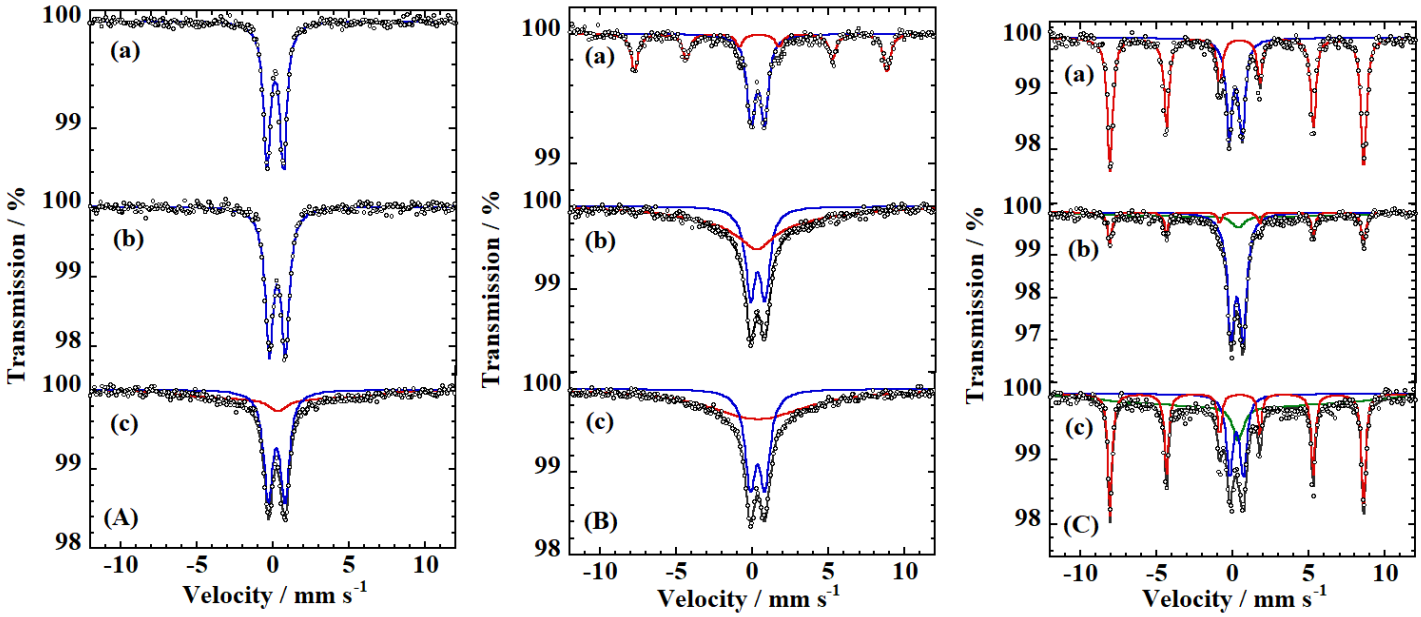


193 **Fig. 3** RT Mössbauer spectra of R-NaWSFe*x* sample with '*x*' of (a) 10, (b) 30, and (c) 50
194 (A) before and after heat treatment for 100 min at (B) 800 °C, and (C) 900 °C

195

196 **Table 2** $^{57}$Fe-Mössbauer parameters of R-NaWSFe*x* sample with '*x*' of 10, 30, 50 before
197 and after heat treatment for 100 min at 800 °C, and 900 °C for 100 min

| | *x* | Assignment | *A* % | $\delta$ mm s$^{-1}$ | $\Delta$ mm s$^{-1}$ | $H_{int}$ T | $\Gamma$ mm s$^{-1}$ |
|---|---|---|---|---|---|---|---|
| Before | 10 | $Fe^{III}(T_d)$ | 100 | $0.15_{\pm 0.01}$ | $1.06_{\pm 0.01}$ | — | $0.55_{\pm 0.01}$ |
| | 30 | $Fe^{III}(T_d)$ | 100 | $0.29_{\pm 0.01}$ | $1.04_{\pm 0.01}$ | — | $0.64_{\pm 0.01}$ |
| | 50 | $Fe^{III}(T_d)$ | 59.5 | $0.25_{\pm 0.01}$ | $1.10_{\pm 0.02}$ | — | $0.68_{\pm 0.02}$ |
| | | $Fe^{III}(O_h)M$ | 40.5 | $0.37_{\pm 0.01}$ | $0.00_{\pm 0.01}$ | $37.0_{\pm 2.6}$ | $0.99_{\pm 0.30}$ |
| 800 | 10 | $Fe^{III}(T_d)$ | 56.3 | $0.34_{\pm 0.01}$ | $0.88_{\pm 0.01}$ | — | $0.62_{\pm 0.01}$ |
| | | $Fe^{III}(O_h)$ | 43.7 | $0.49_{\pm 0.01}$ | $0.10_{\pm 0.02}$ | $51.4_{\pm 0.1}$ | $0.54_{\pm 0.03}$ |
| | 30 | $Fe^{III}(T_d)$ | 38.3 | $0.34_{\pm 0.01}$ | $0.95_{\pm 0.01}$ | — | $0.76_{\pm 0.03}$ |
| | | $Fe^{III}(T_d)$ | 61.7 | $0.27_{\pm 0.12}$ | $0.00_{\pm 0.01}$ | $48.0_{\pm 0.1}$ | $1.83_{\pm 0.88}$ |
| | 50 | $Fe^{III}(T_d)$ | 38.2 | $0.34_{\pm 0.01}$ | $0.95_{\pm 0.01}$ | — | $0.82_{\pm 0.03}$ |
| | | $Fe^{III}(T_d)$ | 61.8 | $0.37_{\pm 0.01}$ | $0.00_{\pm 0.01}$ | $48.2_{\pm 0.1}$ | $7.71_{\pm 0.96}$ |
| 900 | 10 | $Fe^{III}(T_d)$ | 30.3 | $0.19_{\pm 0.01}$ | $0.83_{\pm 0.01}$ | — | $0.49_{\pm 0.01}$ |

| | | | | | | | |
|---|---|---|---|---|---|---|---|
| | | $Fe^{III}(O_h)H$ | 69.7 | $0.38_{\pm0.01}$ | $-0.20_{\pm0.01}$ | $51.6_{\pm0.02}$ | $0.40_{\pm0.01}$ |
| | 30 | $Fe^{III}(T_d)$ | 58.1 | $0.29_{\pm0.01}$ | $0.78_{\pm0.01}$ | — | $0.58_{\pm0.01}$ |
| | | $Fe^{III}(O_h)H$ | 16.3 | $0.37_{\pm0.01}$ | $-0.20_{\pm0.01}$ | $51.7_{\pm0.05}$ | $0.30_{\pm0.02}$ |
| | | $Fe^{III}(O_h)H$ | 25.6 | $0.37_{\pm0.01}$ | $-0.20_{\pm0.01}$ | $51.2_{\pm0.01}$ | $0.29_{\pm0.01}$ |
| | 50 | $Fe^{III}(T_d)$ | 20.1 | $0.26_{\pm0.01}$ | $0.89_{\pm0.02}$ | — | $0.51_{\pm0.03}$ |
| | | $Fe^{III}(O_h)H$ | 37.3 | $0.38_{\pm0.01}$ | $-0.20_{\pm0.01}$ | $51.7_{\pm0.02}$ | $0.31_{\pm0.01}$ |
| | | $Fe^{III}(O_h)H$ | 42.6 | $0.37_{\pm0.01}$ | $-0.20_{\pm0.01}$ | $50.2_{\pm1.91}$ | $0.31_{\pm0.07}$ |

198 *A*: absorption area (±0.5 %), M: γ-$Fe_2O_3$, H: α-$Fe_2O_3$

199

200 $^{57}$Fe-Mössbauer spectra recorded at room temperature and the corresponding
201 parameters of R-NaWSFe*x* sample before and after heat-treatment for 100 min at 800 $^{o}$C
202 and 900 $^{o}$C were shown in Fig. 3 and Table 2, respectively. As shown in Fig. 3 (A) (a)-
203 (c), $^{57}$Fe-Mössbauer spectra of R-NaWSFe*x* before the heat treatment are composed of
204 one paramagnetic doublet with an isomer shift ($\delta$) of (0.15±0.01) − (0.25±0.01) mm $s^{-1}$
205 and quadrupole splitting ($\Delta$) of (1.04±0.01) −(1.10±0.02) mm $s^{-1}$ due to distorted
206 $Fe^{III}O_4$ tetrahedra. An additional relaxed component with $\delta$ of (0.37±0.01) mm $s^{-1}$ and
207 an internal magnetic field ($H_{int}$) of (37.0±2.6) T due to iron oxide nanoparticles was
208 observed for R-NaWSFe50 (Fig. 3 (A) (c)). The $^{57}$Fe-Mössbauer spectrum of R-
209 NaWSFe10 after heat treatment for 100 min at 800 $^{o}$C indicated one paramagnetic
210 doublet due to distorted $Fe^{III}O_4$ and a magnetic sextet with $\delta$ of (0.49±0.01) mm $s^{-1}$, $H_{int}$
211 of (51.4±0.1) T and $\Gamma$ of (0.54±0.03) mm $s^{-1}$ due to regular α-$Fe_2O_3$. A sextet with
212 similar parameters attributed to α-$Fe_2O_3$ were observed for all the Mössbauer of R-
213 NaWSFe*x* heat-treated at 900 $^{o}$, as shown in Fig. 3 (C) (a)-(c). These results are
214 consistent with those of corresponding XRD patterns. However, there are several
215 components which are not clearly identified for the crystalline phase of iron oxide.
216 Therefore, low-temperature Mössbauer measurement was required in order to
217 characterize these components.

218

### 3.3.2 LNT $^{57}$Fe-Mössbauer Spectra

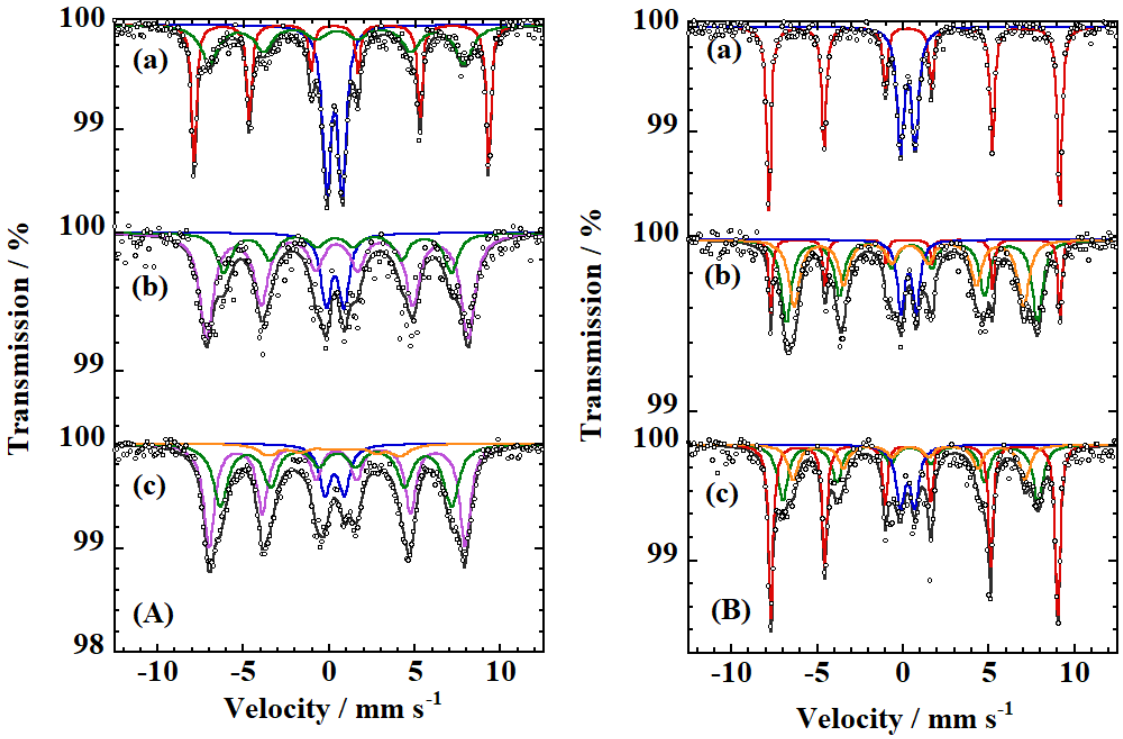


**Fig. 4** Mössbauer spectra measured at 77 K of R-NaWSFe*x* sample with '*x*' of (a) 10, (b) 30 and (c) 50 after heat treatment for 100 min at (A) 800 $^{o}$C and (B) 900 $^{o}$C

**Table 3** Mössbauer parameters at 77 K of R-NaWSFe*x* sample after heat treatment for 100 min at 800 $^{o}$C and 900 $^{o}$C

| | *x* | Assignment | *A* % | $\delta$ mm s$^{-1}$ | $\Delta$ mm s$^{-1}$ | $H_{int}$ T | $\Gamma$ mm s$^{-1}$ |
|---|---|---|---|---|---|---|---|
| 800 | 10 | $Fe^{III}(T_d)$ | 32.1 | $0.29_{\pm0.01}$ | $0.90_{\pm0.01}$ | — | $0.56_{\pm0.02}$ |
| | | $Fe^{III}(O_h)H$ | 34.9 | $0.49_{\pm0.01}$ | $0.39_{\pm0.01}$ | $53.4_{\pm0.1}$ | $0.33_{\pm0.01}$ |
| | | $Fe^{III}(O_h)$ | 33.0 | $0.44_{\pm0.03}$ | $-0.04_{\pm0.06}$ | $46.1_{\pm0.1}$ | $1.20_{\pm0.10}$ |
| | 30 | $Fe^{III}(T_d)$ | 15.2 | $0.32_{\pm0.03}$ | $1.04_{\pm0.05}$ | — | $0.70_{\pm0.10}$ |
| | | $Fe^{III}(O_h)C$ | 61.8 | $0.44_{\pm0.02}$ | $0.03_{\pm0.04}$ | $47.4_{\pm0.1}$ | $0.95_{\pm0.07}$ |
| | | $Fe^{III}(T_d)$ | 23.1 | $0.42_{\pm0.05}$ | $0.13_{\pm0.01}$ | $41.1_{\pm0.05}$ | $0.95_{\pm0.02}$ |
| | 50 | $Fe^{III}(T_d)$ | 10.7 | $0.31_{\pm0.02}$ | $1.12_{\pm0.04}$ | — | $0.77_{\pm0.06}$ |
| | | $Fe^{III}(O_h)C$ | 45.0 | $0.43_{\pm0.01}$ | $0.03_{\pm0.02}$ | $46.4_{\pm0.1}$ | $0.75_{\pm0.04}$ |

| | | | | | | | |
|---|---|---|---|---|---|---|---|
| | | $Fe^{III}(T_d)$ | 36.2 | $0.43_{\pm0.02}$ | $-0.10_{\pm0.04}$ | $41.9_{\pm 0.2}$ | $1.01_{\pm0.07}$ |
| | | $Fe^{III}(T_d)$ | 8.1 | $0.43_{\pm0.01}$ | $-0.22_{\pm 0.24}$ | $24.0_{\pm0.7}$ | $1.27_{\pm0.4}$ |
| 900 | 10 | $Fe^{III}(T_d)$ | 32.7 | $0.28_{\pm0.01}$ | $0.86_{\pm 0.01}$ | - | $0.48_{\pm 0.02}$ |
| | | $Fe^{III}(O_h)H$ | 67.3 | $0.47_{\pm 0.01}$ | $0.35_{\pm0.01}$ | $52.7_{\pm 0.1}$ | $0.32_{\pm0.01}$ |
| | 30 | $Fe^{III}(T_d)$ | 12.1 | $0.33_{\pm0.02}$ | $0.90_{\pm0.03}$ | - | $0.50_{\pm0.04}$ |
| | | $Fe^{III}(O_h)H$ | 13.0 | $0.52_{\pm0.01}$ | $0.37_{\pm0.02}$ | $52.4_{\pm 0.1}$ | $0.25_{\pm0.02}$ |
| | | $Fe^{III}(O_h)C$ | 40.5 | $0.51_{\pm0.01}$ | $-0.01_{\pm0.02}$ | $45.5_{\pm0.1}$ | $0.71_{\pm0.05}$ |
| | | $Fe^{III}(T_d)$ | 34.4 | $0.37_{\pm0.02}$ | $-0.08_{\pm0.03}$ | $41.5_{\pm0.2}$ | $0.75_{\pm0.06}$ |
| | 50 | $Fe^{III}(T_d)$ | 12.6 | $0.26_{\pm 0.03}$ | $0.84_{\pm0.04}$ | - | $0.60_{\pm0.07}$ |
| | | $Fe^{III}(O_h)H$ | 42.1 | $0.46_{\pm 0.01}$ | $0.38_{\pm0.01}$ | $52.0_{\pm0.1}$ | $0.32_{\pm0.02}$ |
| | | $Fe^{III}(O_h)C$ | 27.7 | $0.44_{\pm 0.02}$ | $-0.02_{\pm0.05}$ | $46.3_{\pm0.2}$ | $0.69_{\pm0.07}$ |
| | | $Fe^{III}(T_d)$ | 17.6 | $0.39_{\pm 0.04}$ | $-0.10_{\pm0.07}$ | $42.0_{\pm0.1}$ | $0.69_{\pm0.07}$ |

*A*: absorption area (±0.5 %), H: α-$Fe_2O_3$, C: $CaFe_2O_4$

$^{57}$Fe-Mössbauer spectra measured at 77 K and the corresponding parameters for R-NaWSFe*x* sample with '*x*' of 10, 30 and 50 heat-treated for 100 min at 800 $^{o}$C and 900 $^{o}$C are indicated in Fig. 4 and Table 3, respectively. When in the case of the 77 K $^{57}$Fe-Mössbauer spectrum of R-NaSWFe10 heat-treated at 800 $^{o}$C, one paramagnetic doublet with $\delta$ of (0.29±0.01) mm s$^{-1}$ and $\Delta$ of (0.90±0.01) mm s$^{-1}$ due to $Fe^{III}O_4$ tetrahedra substituting for $Si^{IV}O_4$, and two sextets with $\delta$ and $H_{int}$ of (0.49±0.01) mm s$^{-1}$ and (53.4 ±0.1) T due to α-$Fe_2O_3$, and (0.44±0.03) mm s$^{-1}$ and (46.1 ±0.1) T iron oxide nanoparticles were observed. It is noted that the positive $\Delta$ value of (0.39±0.01) mm s$^{-1}$ observed for 77 K Mössbauer spectrum of R-NaWSFe10 is due to Morin transition occurred at 260 K[11], which is also confirmed for 77 K Mössbauer spectrum of R-NaWSFe heat-treated at 900 $^{o}$C indicating the existence of α-$Fe_2O_3$ in the XRD patterns (Fig. 2 (C)). In addition to a paramagnetic component and two magnetic sextets observed in the 77 K Mössbauer spectrum of R-NaWSFe10, additional one sextet was observed for LNT Mössbauer spectrum of NaWSFe30, and two sextets for NaWSFe50, respectively.

On the other hand, a paramagnetic doublet with $\delta$ of $(0.26 \pm 0.03) - (0.33 \pm 0.02)$ mm $s^{-1}$ and $\Delta$ of $(0.84 \pm 0.04) - (0.90 \pm 0.03)$ mm $s^{-1}$ due to $Fe^{III}O_4$ tetrahedra and a magnetic sextet with $\delta$ of $(0.46 \pm 0.01) - (0.51 \pm 0.02)$ mm $s^{-1}$, internal magnetic field ($H_{int}$) of $(52.0 \pm 0.1) - (52.7 \pm 0.1)$ T and line width ($\Gamma$) of $(0.25 \pm 0.02) - (0.32 \pm 0.02)$ mm $s^{-1}$ due to $\alpha$-$Fe_2O_3$ were commonly found for Mössbauer spectra of R-NaWSFe*x* heat-treated at 900 $^oC$ measured at 77 K. The larger $H_{int}$ value obtained in this study is caused by weak ferromagnetic interaction due to lowering of Morin transition temperature. A similar Mössbauer spectrum with $\delta$ of 0.49 mm $s^{-1}$ and $H_{int}$ of 53.5 T measured at 4.2 K was previously reported for $\alpha$-$Fe_2O_3$ with the particle size of smaller than 20 nm [12]. In addition to these two components, two magnetic sextets with $\delta$ and $H_{int}$ of $(0.51 \pm 0.01)$ mm $s^{-1}$ and $(45.5 \pm 0.1)$ T due to $CaFe_2O_4$[13], and $(0.37 \pm 0.02)$ mm $s^{-1}$ and $(41.5 \pm 0.2)$ T due to iron oxide nanoparticles with unknown structure are observed for 77 K Mössbauer spectrum of R-NaWSFe30 heat-treated at 900 $^oC$. Smaller absorption area (*A*) of 27.7 % due to $CaFe_2O_4$ and 17.6 % of unknown iron oxide nanoparticles were observed for 77 K Mössbauer spectrum of R-NaWSFe50 heat-treated at 900 $^oC$. In the evaluation of *k* values for the MB decomposition by using heat-treated R-NaWSFe*x*, the largest value of $(9.75 \pm 0.01) \cdot 10^{-3}$ $min^{-1}$ was obtained when R-NaWSFe30 heat-treated at 900 $^oC$ was used. It was reported that the band gap energy of $CaFe_2O_4$ of 1.85-1.90 eV[14,15] is slightly smaller than that of $\alpha$-$Fe_2O_3$(1.9-2.2 eV)[16,17]. By considering together this information with the above-described results of Mössbauer and UV-Vis studies, it can be said that the existence of nanoparticles of $CaFe_2O_4$ cause the increase of *k* value in addition to $\alpha$-$Fe_2O_3$. It is concluded that iron oxide nanoparticles precipitated in aluminosilicate are essential for exhibiting visible-light activated photocatalytic effect.

## Conclusions

The largest pseudo-first-order rate constant (*k*) of $9.75 \cdot 10^{-3}$ $min^{-1}$ was recorded for methylene blue degradation test by using R-NaWSFe30 heat-treated at 900 $^oC$ for 100 min under visible-light irradiation. 77 K $^{57}$Fe-Mössbauer spectrum of this sample

revealed the existence of nanoparticles of $CaFe_2O_4$, which was essential for the visible-light activated photocatalytic effect. It is concluded that visible-light activated photocatalyst can be prepared from ubiquitous elements of Na, Al, Si, O, Ca, and Fe. This paper implies that solid waste such as domestic slag which contains above-described elements can be recycled as wastewater purifying material in the future.

## Acknowledgments

Some of the authors (ASA, SI, KN, and SK) express their gratitude for the financial support from Tokyo Human Resources Fund for City Diplomacy.

## References

[1] OECD (2010) "Municipal waste" in OECD Factbook 2010: Economic, Environmental and Social Statistics. OECD Publishing, Paris. DOI: 10.1787/factbook-2010-en.

[2] OECD (2016) "Municipal waste" in OECD Factbook 2015-2016: Economic, Environmental and Social Statistics. OECD Publishing, Paris. DOI: 10.1787/factbook-2015-en.

[3] Annual Report on the Environment, the Sound Material-Cycle Society and Biodiversity in Japan 2018. http://www.env.go.jp/en/wpaper/2018/pdf/07.pdf, Accessed 1 July 2019

[4] Kubuki S, Kawakami N, Kamikawa T, Fukagawa M, Nishizumi T, Nishida T, Homonnay Z, Kuzmann E (2005) Corelationship between local structure and water purifying ability of iron-containing waste glasses. Hyperfine Interact. 166: 429-436

[5] Kubuki S, Iwanuma J, Akiyama K, Homonnay Z, Kuzmann E, Nishida T (2013) Water cleaning ability and local structure of iron-containing soda-lime silicate glass. Hyperfine Interact. 218:41-45.

[6] Kubuki S, Iwanuma J, Takahashi Y, Akiyama K, Homonnay Z, Sinkó K,

Kuzmann E, Nishida T (2014) Visible light-activated catalytic effect of iron-containing soda-lime silicate glass characterized by $^{57}$Fe-Mössbauer spectroscopy. J. Radioanal. Nucl. Chem. 301:1–7

[7] Iida Y, Akiyama K, Kobzi B, Sinkó K, Homonnay Z, Kuzmann E, Ristić M, Krehula S, Nishida T, Kubuki S (2015) Structural analysis and visible light-activated photocatalytic activity of iron-containing soda-lime aluminosilicate glass. J. Alloys Comp. 645:1–6

[8] Ishikawa S, Kobzi B, Sunakawa K, Nemeth S, Lengyel A, Kuzmann E, Homonnay Z., Nishida T, Kubuki S (2017) Visible-light activated photocatalytic effect of glass and glass-ceramic prepared by recycling waste slag with hematite. Pure Appl. Chem. 89(4): 535-544

[9] Wakasa M, Kobayashi Y, Okano M (2006) Magnetic Field Effect on the Photocatalytic Reaction with $TiO_2$ Semiconductor Film. Bull. Soc. Sci. Photo. Jpn. 69(4) 271-275 (in Japanese)

[10] Scherrer P (1918) Bestimmung der Größe und der inneren Struktur von Kolloidteilchen mittels Röntgenstrahlen. Göttinger Nachrichten Gesell. 2:98-100 (in Germany)

[11] F. Van der Wurde (1967) Mössbaeur effect in $\alpha$-$Fe_2O_3$. Physica Status Solidi (b) 17(1): 417- 432

[12] Murad E, Johnston J. H. (1984) In: Long G. J. (ed) Mössbauer Spectroscopy Applied to Inorganic Chemistry, Vol. 2, Plenum Press, New York, pp. 523-531

[13] Hirabayashi D, Sakai Y, Yoshikawa T, Mochizuki K, Kojima Y, Suzuki K, Ohshita K, Watanabe Y (2006) Mössbauer characterization of calcium-ferrite oxides prepared by calcining $Fe_2O_3$ and CaO. Hyperfine Interact. 167(1-3):809-813

[14] Matsumoto Y, Omae M, Sugiyama K, Sato E. I (1987) New photocathode materials for hydrogen evolution: $CaFe_2O_4$ and $Sr_7Fe_{10}O_{22}$. J. Phys. Chem. 91(3): 577–581

[15] Matsumoto Y, Sugiyama K, Sato E. I (1988) Improvement of $CaFe_2O_4$ photocathode by doping with Na and Mg. J. Solid State Chem. 74(1): 117–125

[16] Sivula K, Le Formal F, Grätzel M (2011) Solar Water Splitting: Progress Using Hematite ($\alpha$-$Fe_2O_3$) Photoelectrodes. ChemSusChem, 4: 432−449.

[17] Iandolo B, Wickman B, Zorić I, Hellman A (2015) The Rise of Hematite: Origin and Strategies to Reduce the High Onset Potential for the Oxygen Evolution Reaction. J. Mater. Chem. A 3: 16896− 16912.